Tryptanthrin from indigo: Synthesis, excited state deactivation routes and efficient singlet oxygen sensitization

Daniela Pinheiro [a], Marta Pineiro [a], João Pina [a], Pedro Brandão [a,b], Adelino M. Galvão [c], J. Sérgio Seixas de Melo [a,*]

[a] CQC, Department of Chemistry, University of Coimbra, Rua Larga, 3004-535 Coimbra, Portugal
[b] Department of Chemistry and Centro de Química de Évora - LAQV-REQUIMTE, University of Évora, 7000-671 Évora, Portugal
[c] Centro de Química Estrutural, Instituto Superior Técnico (IST), Universidade de Lisboa, Lisboa, Portugal

A B S T R A C T

The microwave-assisted synthesis of tryptanthrin from indigo in mild oxidation conditions, and a comprehensive study of the excited state properties of this compound in a variety of solvents with different polarity and viscosity values at room and low temperatures are reported. In contrast with indigo, emission of the triplet state of tryptanthrin is observed with a very efficient singlet oxygen sensitization quantum yield, indicating that the triplet state is efficiently populated. From time-resolved fluorescence and femtosecond transient absorption data, further supported with time-dependent density functional theory (TDDFT) calculations, two species, with S_1 states with locally excited (LE) of π,π^* nature and a charge transfer (CT) of n,π^* characteristics, originated from an initially populated Frank-Condon S_2 state (π,π^*), are observed. The two electronically independent species are energetically nearly degenerate and inter-conversion is predicted (and rate constants determined) to occur between LE (S_1) and CT (S_1) species. Due to the low value of the fluorescence quantum yield ($\sim 10^{-3}$) and high triplet state yield ($\phi_T \geq \phi_\Delta$), the high stability of this compound is associated to the high efficiency of the radiationless deactivation processes which involve the formation of the CT state which efficiently converts, through $S_1 \leadsto T_n$ intersystem crossing, to the T_1 triplet state.

1. Introduction

Indigo, an iconic molecule of color [1–5] with a splendid blue color and many natural and synthetic derivatives [6–10] is also the synthetic precursor of tryptanthrin (denoted as **TRYP**). Although with a pale yellowish color, **TRYP** (indolo[2,1-*b*]quinazoline-6,12-dione) (Scheme 1) has gained relevance in the past decades. **TRYP** is a weakly basic indoloquinazoline alkaloid isolated from various natural sources [11], including indigo plants [12,13], fruits [14] and mammals (e.g. urine of Asian elephant) [15,16].

TRYP is known for exhibiting several biological and pharmacological activities including antipathogenic, antifungal, antiparasitic, antituberculosis, antimalarial, anticancer, antioxidant and antiinflammatory [17–23]. Due to the scarcity of the natural existence of **TRYP,** together with its unique bioactive properties, the synthesis of this compound has generated great interest with the development of several synthetic strategies reported [14,17,24–28], such as the oxidation of indigo or the cyclization of isatin and isatoic anhydride [16,29]. Despite

these studies, significant synthetic challenges still remain, since many of these methods are burdensome and are not environmentally friendly [13,16,26,27,29,30]. Therefore the development of a new efficient, low cost, one-pot protocol to access **TRYP** is both attractive and valuable.

In recent years, several tryptanthrin derivatives have been synthesized and studied for their potential optical applications, such as their use as fluorescent chemosensors for metal ions and their potential as dyes in fluorescent imaging. Successful fluorescent imaging in cells and tissues requires the application of dyes which absorb and emit in the "optical window" (concerning the near-infrared (NIR) region of the electromagnetic spectrum – 650–900 nm). This selectivity is required to avoid the interference of endogenous substances during the fluorescent imaging process, as well as to improve tissue penetration levels [30–35].

Recent studies of tryptanthrin derivatives with high fluorescence quantum yields have been reported [21,36,37]. However, only a small number of works describe optical (absorption and fluorescence) properties of **TRYP** itself, highlighting some of its more emissive derivatives [38]. Indeed, Kawakami and co-workers reported that
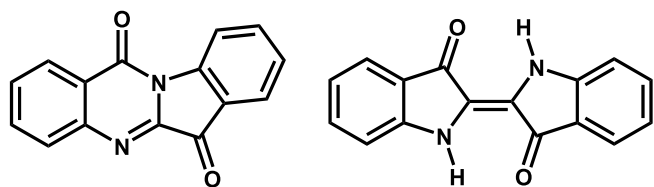
---

* Corresponding author.
  E-mail address: sseixas@ci.uc.pt (J.S. Seixas de Melo).

Scheme 1. Structures of **TRYP** (left) and indigo (right).

2-aminotryptanthrin, when compared with other tryptanthrin derivatives, display interesting photophysical properties including broad wavelength absorption and emission bands in the visible region, high fluorescence quantum yield (ϕ_F) and large positive fluorescence solvatochromism. Noteworthy, this fluorescence solvatochromism was attributed to the planar and polar structure of 2-aminotryptanthrin with an intramolecular charge transfer (ICT) involving the carbonyl group of the five-membered ring and the amino group [38].

In this work, **TRYP** obtained *via* a recently described mild reaction condition [39] was thoroughly studied concerning its photophysical properties. To achieve such a goal, we performed a comprehensive electronic spectral and photophysical study in various solvents and temperatures, investigating the properties of the singlet and triplet excited states which are further rationalized with time-dependent density functional theory (TDDFT) calculations.

2. Experimental Section

2.1. Materials

All the reagents for the synthesis, indigo, sodium hydride (60% dispersion in mineral oil stored in a dry box) and 1,2-diodoethane were obtained from commercial sources and used without further purification. The solvents were used as commercial pro analysis (P.A.) quality. For the spectral and photophysical determinations, the solvents used were of spectroscopic or equivalent grade and were used as received.

2.2. Equipment and methods

Microwave-assisted reactions were performed in a CEM Discover S-Class single-mode microwave reactor, featuring continuous temperature, pressure and microwave power monitoring.

Analytical thin-layer chromatography (TLC) was performed on Macherey-Nagel ALUGRAM Xtra silica gel plates with UV_{254} indicator. Visualization was accomplished by an ultraviolet lamp (254 nm). Silica gel column was carried out with silica gel (230–400 mesh).

Nuclear magnetic resonance (NMR) spectra were recorded at room temperature in $CDCl_3$ solutions on a Bruker Avance III spectrometer and a Bruker DRX-400 spectrometer, both operating at 400.13 MHz for ^1H and 100.61 MHz for ^{13}C. Tetramethylsilane (TMS) was used as internal standard.

Gas chromatography-mass spectroscopy (GC-MS) analyses were performed on a Hewlett-Packard 5973 MSD spectrometer, using electron ionization (EI) (70 eV), coupled to a Hewlett-Packard Agilent 6890 chromatography system, equipped with a HP-5 MS column (30 m × 0.25 mm × 0.25 μm) and high-purity helium as carrier gas. The initial temperature of 70 °C was increased to 250 °C at a 15 °C/min rate, and held for 10 min. Then the temperature was increased to 290 °C at a 5 °C/min rate and held for 2 min, giving a total run time of 32 min. The flow of the carrier gas was maintained at 1.33 mL/min. The injector port was set at 250 °C.

High resolution mass spectrometry (HRMS) was performed on a Bruker microTOF-Focus mass spectrometer equipped with an electrospray ionization time-of-flight (ESI-TOF) source, and is given in Figure SI1.

Absorption and fluorescence spectra were recorded on a Shimadzu

UV-2450 and Horiba-Jobin-Ivon SPEX Fluorolog 3–22 spectrometers respectively. Fluorescence spectra were corrected for the wavelength response of the system.

The singlet extinction coefficients (ε_{ss}) were obtained from the slope of the plot of the absorption with (at least) five solutions of different concentrations versus the concentration (correlation values > 0.999).

The fluorescence quantum yields (ϕ_F) at room temperature (T = 293 K) were measured using α-quaterthiophene, α4 ($\phi_F = 0.16$) [40] in acetonitrile (MeCN) as standard using the equation below (eq. (1)):

$$\phi_F^{cp} = \frac{\int I^{cp}(\lambda)\, d\lambda}{\int I^{ref}(\lambda)\, d\lambda} \cdot \frac{n_{cp}^2}{n_{ref}^2} \cdot \phi_F^{ref} \tag{1}$$

where ($\int I^{cp}(\lambda)\, d\lambda$) is the integrated area under the emission spectra of the compound (*cp*) solution and $\int I^{ref}(\lambda)\, d\lambda$ of the reference (*ref*) solution, n_{cp}^2 and n_{ref}^2 are the refractive index of the solvents in which the compounds and the reference were respectively dissolved and ϕ_F^{ref} is the fluorescence quantum yield of the standard. The fluorescence quantum yields were obtained with optically matched solutions, at the excitation wavelength, of **TRYP** and α_4.

Phosphorescence measurements were recorded with a Horiba-Jobin-Ivon SPEX Fluorolog 3–22 spectrometer using a 150 W pulsed Xenon lamp. The phosphorescence spectra were corrected for the wavelength response of the system. Phosphorescence experiments were performed with a quartz NMR-like tube. Due to the smaller optical pathway, *l*, an absorbance of ~0.4 (checked with a 1 cm length cuvette) was used in contrast to the ~0.2 used in fluorescence experiments. This tube was put inside a dewar (fixed to the equipment with an appropriate holder) filled up with liquid nitrogen.

The phosphorescence quantum yields were determined using biacetyl ($\phi_{Ph} = 0.23$) [41], in a mixed solvent containing diethyl ether, isopentane and ethanol in a 5:5:2 (v/v/v) ratio as standard [42].

Singlet oxygen formation quantum yields (ϕ_Δ) were obtained by direct measurements of the phosphorescence emission spectra of singlet oxygen, $^1O_2$, centered at 1276 nm with a Horiba-Jobin-Ivon SPEX Fluorolog 3–22 spectrometer equipped with a near-infrared (NIR) detector Hamamatsu R5509-42 photomultiplier cooled to 193 K in a liquid nitrogen chamber. To avoid the overlap of the fluorescence emission second harmonic signal with the sensitized singlet oxygen phosphorescence emission at 1275 nm a Newport longpass dielectric filter with 1000 nm cut-on (reference 10LWF-1000-B) was used. The sensitized phosphorescence emission spectra of $^1O_2$ from optically matched solutions of the samples and that of the reference compound were obtained in identical experimental conditions. The singlet oxygen formation quantum yield was then determined by comparing the integrated area under the emission spectra of the sample solutions ($\int I^{cp}(\lambda)\, d\lambda$) and that of the reference solution ($\int I^{ref}(\lambda)\, d\lambda$) and applying the equation (eq. (2)) [43],

$$\phi_\Delta^{cp} = \frac{\int I^{cp}(\lambda)\, d\lambda}{\int I^{ref}(\lambda)\, d\lambda} \cdot \phi_\Delta^{ref} \tag{2}$$

with ϕ_Δ^{ref} the singlet oxygen formation quantum yield of the reference compound. 1H-phenalen-1-one in acetonitrile ($\phi_\Delta = 0.98$) was used as standard [44]. The singlet oxygen formation quantum yields were obtained with optically matched solutions, at the excitation wavelength, of **TRYP** and 1H-phenalen-1-one.

Fluorescence decays were measured using a home-built picosecond time-correlated single photon counting (ps-TCSPC) apparatus described elsewhere [45]. The excitation source consists of a tunable picosecond Spectra-Physics mode-lock Tsunami laser (Ti:Sapphire) model 3950 (80 MHz repetition rate, tuning range 700–1000 nm), pumped by a 532 nm continuous wave Spectra-Physics Millennia Pro-10s laser. The excitation wavelengths used in this work (409 nm, 411 nm and 422 nm) were obtained with a Spectra-Physics harmonic generator, model GWU-23PS.

The fluorescence decay curves were deconvoluted using the experimental instrument response function signal collected with a scattering solution (aqueous Ludox solution). The deconvolution procedure was performed using the modulation function method, as implemented by G. Striker in the SAND program, and previously reported in the literature [46].

The experimental setup for the ultrafast spectroscopic and kinetics measurements consisted of a broadband (350–1600 nm) HELIOS pump-probe femtosecond transient absorption spectrometer from Ultrafast Systems, pumped by an amplified femtosecond Spectra-Physics Solstice-100F laser (800 nm central wavelength, 128 fs pulse width and 1 kHz repetition rate) and coupled to a Spectra-Physics TOPAS Prime F optical parametric amplifier (195–22000 nm tuning range). The probe light in the UV range was generated by passing a small portion of the 800 nm light from the Solstice-100F laser through a computerized optical delay (with a time window of up to 8 ns) and then focusing in a vertical translating CaF_2 crystal to generate a white-light continuum (350–750 nm). All the measurements were obtained in a 2 mm quartz cuvette, with absorptions of ~0.3 at the pump excitation wavelength. To avoid photodegradation, the solutions were stirred during the experiments or kept in movement with a frequency lower than the laser using a motorized translating sample holder. Background signals from impurities or unwanted coherent effects were ruled out by scans of the neat solvent. The spectral chirp of the data was corrected using Surface Xplorer PRO program from Ultrafast Systems. Global analysis of the data (using a sequential model) was performed using Glotaran software [47].

The experimental setup (applied photophysics laser flash photolysis apparatus pumped by a Spectra-Physics Nd:YAG laser) used to obtain the nanosecond-microsecond transient absorption spectra has been described elsewhere [48,49].

All theoretical calculations were of the density functional theory (DFT) type, carried out using GAMESS-US [50] version R3. A range corrected CAMB3LYP [51] functional, with 65% Hartree-Fock (HF) exact exchange at long range and 19% at short range, was used in both ground- and excited-state calculations. TDDFT calculations, with similar functionals, were used to probe the excited-state potential energy surface (PES). The solvent was included using the polarizable continuum model with the solvation model density to add corrections for cavitation, dispersion, and solvent structure. In TDDFT calculation of FC (Franck-Condon) excitations the dielectric constant of the solvent was split into a "bulk" component and a fast component, which is essentially the square of the refractive index [52]. In "adiabatic" conditions only the static dielectric constant is used. A 6-31G** basis set was used in either DFT or TDDFT calculations. CAMB3LYP slightly overestimates excitations with a scaling correction applied to the reported values ($E_{reported} = E_{TDDFT} \times 0.92 - 0.19$) [6]. Excitations were corrected for zero point vibrational energy by using, essentially, the frequency of the relaxing vibrational mode (± 0.06 eV). Triplet energetics was estimated from UHF CAM-B3LYP calculations with multiplicities of 1 and 3.

2.3. Synthesis of tryptanthrin

In a glass microwave reactor charged with a magnetic stirring bar, indigo (100 mg, 1 equiv.) and sodium hydride (NaH) (2 equiv.) were dissolved in 1 mL of *N,N'*-dimethylformamide (DMF). The 1,2-diodo-ethane was added (2 equiv.) and solvent was added to a total volume of 2 mL. The resulting mixture was heated under microwave (MW) irradiation at 50 °C for 15 min. After cooling down to room temperature, a sample was collected, dissolved in 1 mL of dichloromethane and washed with 1 mL of water. The organic layer was analyzed by GC-MS and the analysis of the reaction media showed the presence of isatin, isatoic anhydride, tryptanthrin and unreacted indigo [39]. The crude was extracted with dichloromethane and isolated by column chromatography (SiO_2) using hexane:ethyl acetate (8:2) as eluent to yield pure **TRYP** (yellow solid; 25 mg; yield: 26%). The chemical structure of tryptanthrin was confirmed by GC-MS and HRMS analysis as well ^{1}H and

[13]C spectroscopy.

^{1}H NMR ($CDCl_3$, 400 MHz), δ (ppm): 8.61 (d, $J = 8.1$ Hz, 1H, ArH), 8.42 (dd, $J = 7.9$ Hz, $J = 1.3$ Hz, 1H, ArH), 8.02 (d, $J = 7.8$ Hz, 1H, ArH), 7.90 (d, $J = 7.6$ Hz, 1H, ArH), 7.82–7.87 (m, 1H, ArH), 7.76–7.80 (m, 1H, ArH), 7.64–7.68 (m, 1H, ArH), 7.40–7.44 (m, $J = 7.5$ Hz, $J = 0.4$ Hz, 1H, ArH); ^{13}C NMR ($CDCl_3$, 101 MHz) δ (ppm): 182.6 (C=O), 158.1 (C=O), 146.6, 146.4, 144.4, 138.3, 135.1, 130.8, 130.3, 127.6, 127.2, 125.4, 123.8, 122.0, 118.0; GC-MS: m/z [M$^+$] = 248.0; HRMS (ESI-TOF-MS): m/z [M+1]$^+$ = 249.0659 obtained for $C_{15}H_9N_2O_2$ (calc. 249.0659), see SI for further details.

3. Results and discussion

3.1. Synthesis

TRYP was obtained from indigo using a *trio* oxidant system - NaH, an iodine source and DMF - under MW irradiation, as recently described by our group (Scheme 2). Briefly, we verified that under these reaction conditions, indigo is converted to isatin and isatoic anhydride, which further condensate to afford tryptanthrin [39]. This approach is a faster and greener methodology to achieve this compound from indigo, and requires milder conditions when compared with previously described methods.

3.2. Excited state characterization of tryptanthrin

3.2.1. Absorption and steady state fluorescence

The absorption, fluorescence emission and excitation spectra of **TRYP** were obtained at T = 293 K, in six organic solvents with different dielectric constant (ε) and in a viscous mixture of methanol:glycerol (70:30, v/v). The solvents polarity ranged from $\varepsilon = 1.84$ (n-pentane) to $\varepsilon = 36.71$ (DMF) see Table 1. The absorption, excitation and fluorescence emission spectra of **TRYP** in dichloromethane (DCM) (moderately polar aprotic solvent), MeCN (polar aprotic solvent) and methanol (MeOH) (polar protic solvent) at T = 293 K are depicted in Fig. 1.

Fig. 1 shows that the emission band is strongly red-shifted relative to the longest wavelength absorption band. The emission is also solvent dependent as seen in Fig. 1 by the red-shifting with the solvent polarity. It can also be observed a good overlap between the absorption and the excitation spectra, thus attesting the purity of **TRYP**.

Table 1 summarizes the spectral (absorption and emission) data for **TRYP** in the investigated solvents and that of indigo in DMF for comparison. Observation of data in Table 1 shows several interesting features: (i) the absorption spectra are relatively unaffected by changes in solvent polarity and by differences in the hydrogen bonding ability of the alcoholic solvents; (ii) the red-shift of the emission wavelength band; (iii) the high dependence of the emission band with the solvent polarity; (iv) the high Stokes shift (Δ_{SS}) in protic alcohols, thus supporting the occurrence of an excited state charge transfer state; (v) the significant blue shift of **TRYP**, both in the absorption and fluorescence emission maxima, relative to indigo and (vi) the much lower molar extinction coefficient values of **TRYP** relative to indigo. The molar absorption coefficients (ε_{SS}) are, however, of the same order of magnitude ($\varepsilon_{SS} \approx 10^3$ M^{-1} cm^{-1}) of previously reported values for **TRYP** derivatives [32,36].

To further evaluate the effect of the solvent on the fluorescence emission (excited state interactions) of **TRYP**, the Stokes shift has been plotted against the Dimroth-Reichardt E_T^N polarity parameter [55]. This plot is shown in Figure SI2 and found to display a linear dependence of Δ_{SS} *vs.* E_T^N, thus indicating that solute-solvent dipole–dipole interactions are mainly responsible for the solvent-dependent observed fluorescence shift [56,57]. The nature of the charge transfer singlet excited state will be further discussed at the light of the TDDFT calculations.

3.2.2. Photophysical data

A summary of the photophysical parameters, obtained in different
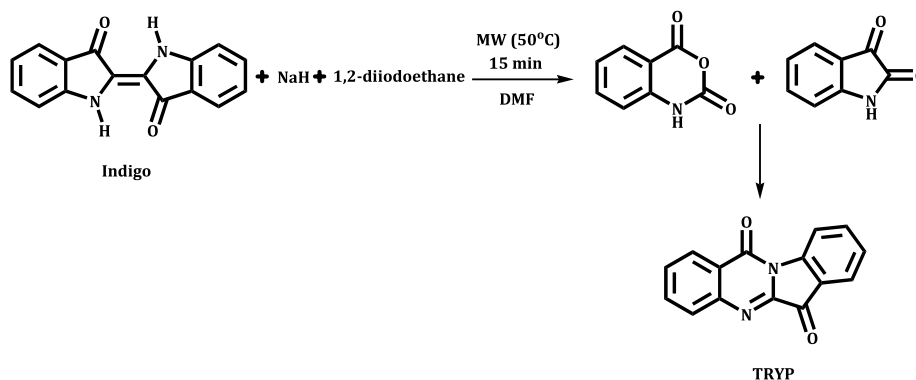
Scheme 2. Schematic synthetic pathway for the synthesis of **TRYP** from indigo.

Table 1
Spectral data including absorption (λ_{Abs}), fluorescence (λ_{Fluo}) and phosphorescence (λ_{Ph}) wavelength maxima, Stokes shifts ($\triangle_{SS}$), molar extinction coefficient (ε_{SS}) and singlet (E_S) and triplet (E_T) state energies for **TRYP** in different solvents at T = 293 K. For indigo the same parameters are also presented in DMF for comparison.

Compound	Solvent	η^b (cP)	ε	λ_{Abs} (nm)	λ_{Fluo} (nm)	$\Delta_{SS}{}^c$ (cm^{-1})	$\varepsilon_{SS}{}^d$ (M^{-1} cm^{-1})	E_S (eV)	λ_{Ph} (nm)	E_T (eV)	$\Delta E_{S\text{-}T}$ (eV)
Indigo[a]	DMF	0.924	36.71	610	653	1080	22140	1.97	–	–	0.91[e]
TRYP	n-pentane	0.214	1.84	390	506	5878	1553	2.90	N.D.[f]	N.D.[f]	N.D.[f]
	DCM	0.410	8.93	399	508	5378	6623	2.81	N.D.[f]	N.D.[f]	N.D.[f]
	MeCN	0.345	35.94	394	513	5888	3545	2.79	N.D.[f]	N.D.[f]	N.D.[f]
	DMF	0.924	36.71	394	514	5925	3576	2.78	N.D.[f]	N.D.[f]	N.D.[f]
	EtOH	1.200	24.55	389	539	7154	4169	2.84	567, 615	2.39	0.45
	MeOH	0.593	32.66	389	552	7591	3736	2.78	N.D.[f]	N.D.[f]	N.D.[f]
	MeOH:Glycerol (70:30)	7.700[g]	36.70[g]	391	551	7427	3527	2.76	N.D.[f]	N.D.[f]	N.D.[f]

[a] For indigo in DMF data from Ref. [4].
[b] η = Viscosity.
[c] Δ_{SS} = Stokes shifts.
[d] ε_{SS} = Molar extinction coefficient.
[e] Data taken from Ref. [53].
[f] N.D. = Not determined.
[g] For MeOH:Glycerol 70:30 vol ratio data from Ref. [54].

solvents, including fluorescence, phosphorescence, intersystem crossing triplet and internal conversion quantum yields, lifetimes and rate constants for the radiative and radiationless processes, is given in Table 2.

Observation of Table 2 shows that the fluorescence quantum yield is higher in MeCN and DMF than in the polar protic solvents, MeOH and ethanol (EtOH) and in the methanol:glycerol (70:30, v/v) mixture studied. The fluorescence lifetimes also show a gradual decrease on going from polar aprotic to protic solvents. Noteworthy is the highly efficient singlet oxygen sensitization of **TRYP** in aerated MeCN solution, $\phi_\Delta = 0.77$ (see Figure SI3 and Table 2), which establishes the $S_1 \leadsto T_1$ as the dominant deactivation channel, clearly contrasting with indigo where the $S_1 \leadsto S_0$ (internal conversion) is the dominant deactivation channel with more than 99.99% of the quanta loss occurring from this channel [53,58,59].

Also in contrast to indigo [53,59] and derivatives [4,60], where no phosphorescence emission was observed, in the case of **TRYP** phosphorescence in ethanol glass at 77 K could be observed (see Fig. 2). A broad phosphorescence emission band is observed with two vibronic bands (567 and 615 nm) which partially overlaps the fluorescence emission (also collected at low temperature, 77 K), as illustrated in Figure SI4. A phosphorescence lifetime of 10.3 ms was obtained (see Figure SI5 for the mono-exponential decay profile). This indicates the nature of the triplet state to be of n,π^* origin [61]. The very close proximity with the S_1 (CT), i.e., the small singlet-triplet energy gap of 0.45 eV (see below) further supports the very efficient $S_1 \leadsto T_1$ intersystem crossing deactivation channel [61,62]. In addition, strong triplet-triplet absorption bands were found for **TRYP** (see below), thus giving support for the close proximity of the S_1 and T_1 states.

From the photophysical data in Table 2, and considering that $\phi_T \geq \phi_\Delta$,

it can be observed that the internal conversion deactivation channel (ϕ_{IC}) represents, ca. 22% of the quanta loss (ϕ_{IC} = 1- ϕ_T - ϕ_F).

Due to Franck-Condon forbidden nature of the absorption spectra of **TRYP,** the singlet energy values were obtained from the interception of the normalized absorption (lowest energy band) and the fluorescence emission spectra. The triplet energy value was taken from the energy of the 0-0 vibronic band of the phosphorescence spectra. The obtained singlet-triplet energy gap, $\Delta E_{S\text{-}T}$ = 0.45 eV (3629 cm^{-1}), is lower than the value found for indigo $\Delta E_{S\text{-}T}$ = 0.91 eV (7340 cm^{-1}) [2,53]. The small $\Delta E_{S\text{-}T}$ value found for **TRYP** together with the observed properties of the time-resolved data will be discussed in detail in section 3.2.3.

3.2.3. TDDFT calculations

TDDFT calculations show that the observed lowest absorption band corresponds to an $S_0 \rightarrow S_2$ ($\pi \rightarrow \pi^*$) transition (392 nm). The S_2 state is predicted to have a strong $S_2 \rightarrow S_{14}$ transient absorption at 478 nm (f = 0.38), in agreement with the fs-TA spectroscopic data (see below). Table 3 summarizes the data for the calculated transitions, namely wavelength maxima, λ (nm), oscillator strength (f) and the major contributions of the Molecular Orbitals (MO) of the transitions involved. The calculated UV-VIS and fluorescence spectra are given in Figure SI6.

The frontier orbitals representing the main contributions CT and LE states involving respectively major contributions of n$\rightarrow\pi^*$ and $\pi\rightarrow\pi^*$ transitions are presented in Fig. 3. The CT state mainly results from the transition from the **I** (HOMO-2) to the **III** (LUMO) orbitals (n$\rightarrow\pi^*$ character) whereas the LE mainly results from the transition from **II** (HOMO) to **III** (LUMO) orbitals ($\pi \rightarrow\pi^*$ nature).

In solvents of low polarity values the calculations always end-up with degenerate S_1 and S_2 states. This suggests that a hybrid LE/CT can be
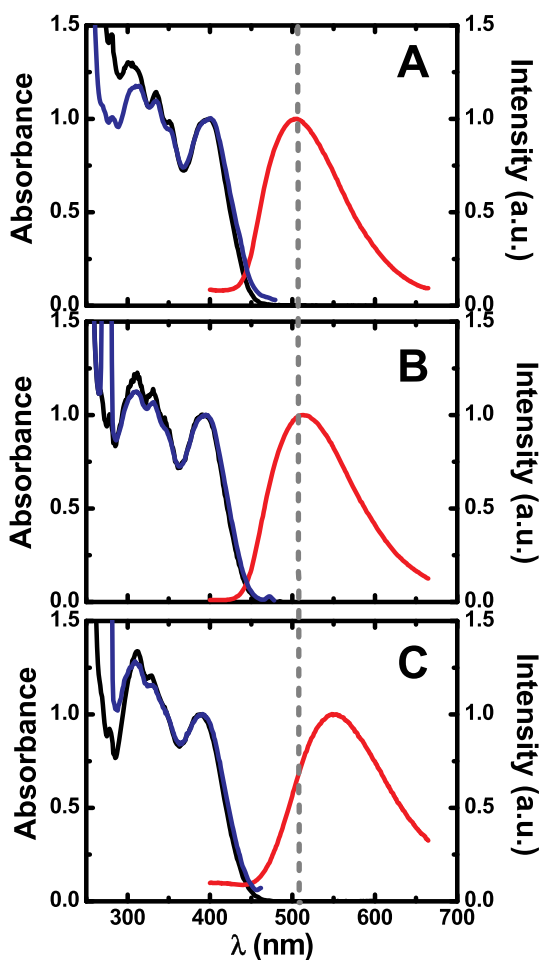
Fig. 1. Normalized absorption (black line), excitation (blue line) and fluorescence emission (red line) spectra in dichloromethane (DCM) (**A**), acetonitrile (MeCN) (**B**) and methanol (MeOH) (**C**) solutions at T = 293 K. Fluorescence emission spectra obtained with excitation wavelength λ_{exc} = 340 nm and the excitation spectra collected with λ_{em} = 505 nm and λ_{em} = 550 nm. The dashed vertical line is just meant to be a guideline for the eye. (For interpretation of the references to color in this figure legend, the reader is referred to the Web version of this article.)

proposed for this system. In gas phase, the calculations show a decrease in the energetic separation between S_1 and S_2, making hybrid LE/CT states more favorable but more difficult to analyze by TDDFT since they may have different sensitivities to the amount of HF exact exchange used in calculations and its ordering reversed.

Nevertheless, in MeCN the LE and CT are clearly distinct states and probing the PES of both the S_1 and S_2 states (in MeCN and gas phase) allowed us to find that the excited state can decay according to two
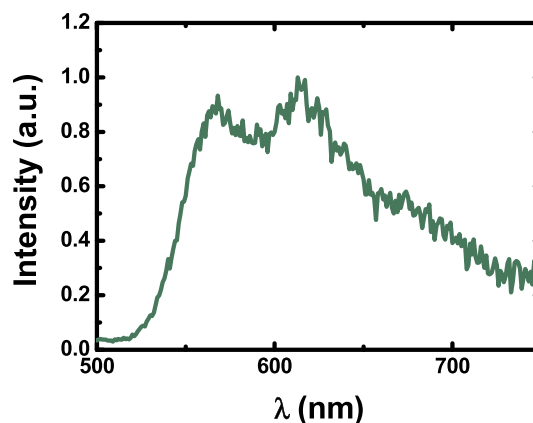
Fig. 2. Phosphorescence spectra for **TRYP** in ethanol at T = 77 K.

Table 3
Predicted singlet and triplet transitions for **TRYP** in the gas phase and in MeCN including the expected wavelength maxima and the orbitals involved in the transition.

Solvent/state	λ (nm)	f	Major orbitals involved in the transition[a]
Gas phase $S_0 \rightarrow S_1$	450	0	HOMO-2 → LUMO (−0.89)
Gas phase $S_0 \rightarrow S_2$	392	0.17	HOMO → LUMO (−0.92)
Gas phase $S_2 \rightarrow S_{14}$	478	0.38	(S_2) HOMO-2 → LUMO (−0.89) (S_{14}) HOMO-7 → LUMO (−0.77)
Gas phase $T_1 \rightarrow S_0$	591	0	b
Gas phase $S_1 \rightarrow S_0$	489	0.08	HOMO → LUMO (0.95)
Acetonitrile $S_1 \rightarrow S_0$	508	0.17	HOMO → LUMO (0.97)

[a] In brackets the coefficient contribution of this transition.
[b] T_1 calculated by DFT as the ground state triplet.

Table 2
Photophysical data including fluorescence (ϕ_F), phosphorescence (ϕ_{Ph}), intersystem crossing triplet (ϕ_T) and internal conversion (ϕ_{IC}) quantum yields, fluorescence (τ_F) and phosphorescence lifetimes (τ_{Ph}) and rate constants (fluorescence (k_F), nonradiative (k_{NR}), internal conversion (k_{IC}) and intersystem crossing (k_{ISC})) for **TRYP** in various solvents at T = 293 K and T = 77 K. For indigo the same parameters are also presented in DMF for comparison.

Compound	Solvent	η[b] (cP)	ε	ϕ_F (293 K)	τ_F (ps)[c] (293 K)	ϕ_{Ph} (77 K)	τ_{Ph} (ms) (77 K)	$\phi_\Delta \approx \phi_T$ (293 K)	ϕ_{IC} (293 K)	k_F (ns^{-1})[d] (293 K)	k_{NR} (ns^{-1})[d] (293 K)	k_{IC} (ns^{-1})[d] (293 K)	k_{ISC} (ns^{-1})[d] (293 K)
Indigo[a]	DMF	0.924	36.71	0.002	135	–	–	0.0066[f]	0.991	0.017	7.390	7.341	0.049
TRYP	MeCN	0.345	35.94	0.008	499			0.77	0.22	0.017	1.987	0.440	1.547
	DMF	0.924	36.71	0.007	368					0.020	2.698		
	EtOH	1.200	24.55	0.003	255	0.0027	10.3			0.011	3.911		
	MeOH	0.593	32.66	0.002	146					0.013	6.836		
	MeOH: Glycerol (70:30)	7.700[e]	36.70[e]	0.002	127					0.015	7.859		

[a] For indigo in DMF data from Ref. [3].
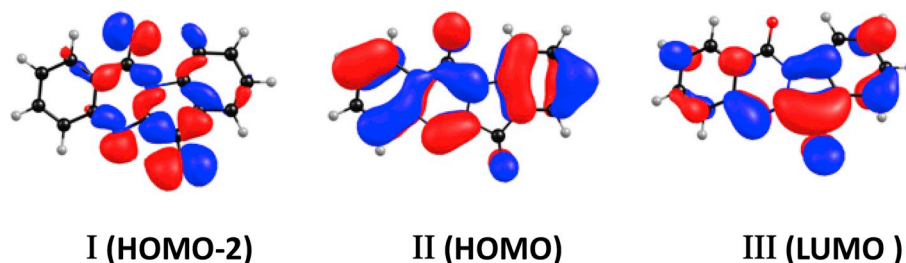[b] η = Viscosity.
[c] The decay time considered here is the slower component in the fluorescence decays.
[d] $k_F = \dfrac{\phi_F}{\tau_F}$; $k_{NR} = \dfrac{(1-\phi_F)}{\tau_F}$; $k_{IC} = \dfrac{1-\phi_F-\phi_T}{\tau_F}$; $k_{ISC} = \dfrac{\phi_T}{\tau_F}$. $\phi_{IC} = 1 - \phi_T - \phi_F$
[e] For MeOH:Glycerol (70/30) volume ratio data from Ref. [54]. [f] Data from Ref. [53].

I (HOMO-2)   **II (HOMO)**   **III (LUMO)**

Fig. 3. Topological plots of n (**I**), π (**II**) and π* (**III**) orbitals of **TRYP**.

different pathways: it relaxes to a CT state of n,π* nature (which can convert to a T_1 state predicted in gas phase at 591 nm, which is in agreement with the phosphorescence first vibronic band at ~ 567 nm (see Fig. 2) and to a LE π,π* emissive state. The later shows a strong emissive dependence with the solvent polarity red-shifting by 19 nm from gas phase (489 nm) to MeCN (508 nm), in agreement with the data in Table 1 and Figure SI2. This effect brings the energy of the emissive state closer to that of the triplet state, therefore increasing the efficiency of the S~~~>T intersystem crossing (ISC) in polar solvents making it the dominant deactivation channel.

Scheme 3 summarizes, conceptually, the results of DFT/TDDFT calculations, used to provide insight on the photophysics of **TRYP**. It is worth noting that in Scheme 3, the xx' and yy' axes are neither to scale nor represent a physical relaxation coordinate. The vibronic levels are not associated to calculated vibrations, with the exception of the lowest vibronic which correspond to the energy minimum corrected to zero point vibrational energy (see Experimental Section).

As explained below, due to the energetic proximity of the states obtained by either pathway (CT and LE), they can interconvert originating double exponential decays in time-resolved fluorescence.

With irradiation of the electronic ground state of **TRYP**, with 392 nm (λ_{pump}), the Frank-Condon state S_2, π,π* is populated (vertical transition) which, within the IRF of the pump-pulse rapidly decays (<250 ps) to S_1

LE (π,π*) that can interconvert to S_1 CT (n,π*) (Scheme 3).

From the fs-TA data analysis in MeCN using a sequential model, it was found that the CT state can be formed at the expenses of the LE state (~8.9 ps rise-time) and depopulates (through ISC to form the triplet state, by fluorescence or by internal conversion to the ground-state) in ~466 ps. This is further corroborated by time-resolved fluorescence. This will be discussed in detailed in the next two sections (3.2.4 and 3.2.5).

3.2.4. Time-resolved fluorescence

Upon excitation to the S_2 state of **TRYP** and rapid vibrational relaxation to S_1 (LE) and S_1 (CT) species whose fluorescence decays (according to Scheme 4) are obtained in a ps time scale (with 4 ps time resolution). These were obtained in different solvents at room temperature, with excitation at 409 nm, 411 nm and 422 nm and collected at different emission wavelengths (Table 4).
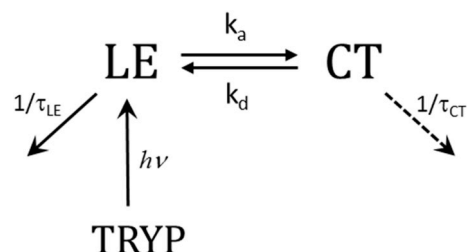
Global analysis of the data revealed that the fluorescence decays are fitted with sums of two exponentials according to eq. (3):
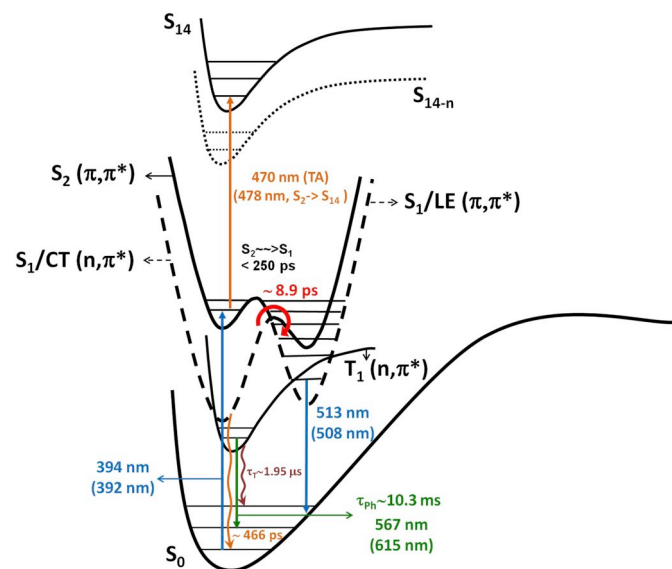
$$I(t) = \sum_{i,j=1}^{2} a_{ij} e^{-t/\tau_i} \tag{3}$$

with identical decay times (τ_i) but different pre-exponential factors (a_{ij}) all over the emission spectra (see Figure SI7). The data reveal that, with exception of MeCN and DMF, at higher energies the shorter decay component dominates, whereas at the tail of the emission band the longer decay components dominates with the shorter component now displaying a negative associated pre-exponential factor, thus corroborating the presence of an excited state dynamic process (LE state giving rise to the CT state).

In the case of indigo, the bi-exponential nature of the decay was found to be consistent with a keto-excited form giving rise to the enol form by single fast proton transfer [3,4]. The presence of the rising component at longer emission wavelengths is particularly relevant for this molecule, and demonstrates that the second species (the longer-lived enol) is formed at the expense of the shorter-lived keto species [2,3]. From Table 4 it can be seen that for **TRYP**, with the exception of MeCN where no rising component is observed, in all the other solvents including the methanol:glycerol mixture a rising component (indicated by the negative pre-exponential value) at the longer wavelength emission is present (Fig. 4).

Therefore, the solution of this 2-state kinetic scheme (see Scheme 4)

Scheme 3. Schematic diagram with potential energy curves for predicted states and transitions resulting from the experimental and TDDFT data for **TRYP** in acetonitrile (MeCN), in gas phase the absorption band is predicted at 392 nm. The values in brackets represent the TDDFT predicted transitions. A S_1–S_{14} transition is predicted from TDDFT and corroborated by fs-TA experiments. The S_2 state rapidly deactivates to the S_1 state. The S_1 (LE) interconverts in 8.9 ps into S_1 (CT) (dashed line), which in 466 ps day to ground state. The triplet state formed, T_1, during the deactivation of S_1, has a phosphorescence lifetime of 10.3 ms.

Scheme 4. Kinetic scheme for the excited behavior of **TRYP** in S_1.

Table 4
Time resolved fluorescence data (lifetimes, τ_i, pre-exponential factors, a_i, and chi-squared values, χ^2) obtained with Picosecond Time-Correlated Single Photon Counting (ps-TCSPC) technique for **TRYP**, collected at different emission wavelengths obtained with λ_{exc} = 409 nm, λ_{exc} = 411 nm and λ_{exc} = 422 nm at T = 293 K. For indigo the same parameters are also presented in DMF for comparison.

Compound	λ_{exc} (nm)	Solvent	λ_{em} (nm)	τ_1 (ps)	τ_2 (ps)	a_1	a_2	χ^2
Indigo[a]	378	DMF	630	10	135	0.61	0.39	1.10
			660			−0.51	1.00	1.03
TRYP	411	MeCN	480	65	499	0.15	0.85	1.06
			510			0.11	0.89	1.16
			630			0.05	0.95	1.12
	409	DMF	480	29	368	0.12	0.88	1.11
			510			0.03	0.97	1.08
			630			−0.03	1.00	1.15
	422	EtOH	490	23	255	0.78	0.22	1.07
			540			0.42	0.59	0.92
			620			−0.27	1.00	0.91
	409	MeOH	500	12	146	0.73	0.27	1.23
			550			0.25	0.75	1.13
			600			−0.48	1.00	1.34
		MeOH:Glycerol (70:30)	500	17	127	0.73	0.27	1.06
			550			0.23	0.77	1.11
			600			−0.35	1.00	1.30

[a] For indigo in DMF data from Ref. [3].

allows one to obtain the kinetic constants for the formation (k_a) and deactivation (k_d) of the CT and LE species [43]. It is worth mentioning that in Scheme 4, the dashed arrow associated with the decay of the CT state/species reflects the fact that this is a dark state and the decay is essentially non-radiative.

The differential equations ruling out the time dependence concentration of the two excited species are, according to Scheme 4, given by [63–65]:

$$\frac{d}{dt}\begin{bmatrix} LE^* \\ CT^* \end{bmatrix} = \begin{bmatrix} -k_X & k_d \\ k_a & -k_Y \end{bmatrix} \cdot \begin{bmatrix} LE^* \\ CT^* \end{bmatrix} \tag{4}$$

where LE* and CT* are the concentrations of S_1(LE) and S_1(CT) in the excited state and k_X and k_Y given by eq. (5) and (6):

$$k_X = k_a + k_{LE} \tag{5}$$

$$k_Y = k_d + k_{CT} \tag{6}$$

Fig. 4. Fluorescence decays of **TRYP** obtained in methanol (MeOH) at T = 293 K. The fluorescence decay times (τ_i) in ps and the associated pre-exponential factors (a_{ij}) are presented in the inset. For a better judgment of the quality of the fits, the weighted residuals, autocorrelation functions (ACs) and chi-squared (χ^2) values are also shown. The dashed lines in the decays are the pulse instrumental response.

where k_{LE} is the reciprocal of the lifetime of the LE species and k_{CT} represents the deactivation of the CT species (since this is a dark state this deactivation essentially mirrors the radiationless process). Integration of eq. (4) leads to

$$\begin{bmatrix} LE^* \\ CT^* \end{bmatrix} = \begin{bmatrix} a_{11} & a_{12} \\ a_{21} & a_{22} \end{bmatrix} \cdot \begin{bmatrix} e^{-\lambda_1 t} \\ e^{-\lambda_2 t} \end{bmatrix} \tag{7}$$

where the eigen values λ_i are the reciprocal decay times of the shorter ($\lambda_2 = 1/\tau_2$) and of the longer ($\lambda_1 = 1/\tau_1$) species and are related to the rate constants in Scheme 4 by the characteristic eq. [66]:

$$\begin{vmatrix} \lambda - k_X & k_d \\ k_a & \lambda - k_Y \end{vmatrix} = 0 \tag{8}$$

the solutions of which are given by eq. (9).

$$2\lambda_{2,1} = (k_X + k_Y) \pm [(k_X - k_Y) + 4k_a k_d]^{1/2} \tag{9}$$

The sum and product of the lambda values (λ_1 and λ_2) resulting from eq. (9) are respectively given by:

$$k_X + k_Y = \lambda_1 + \lambda_2 \tag{10}$$

and

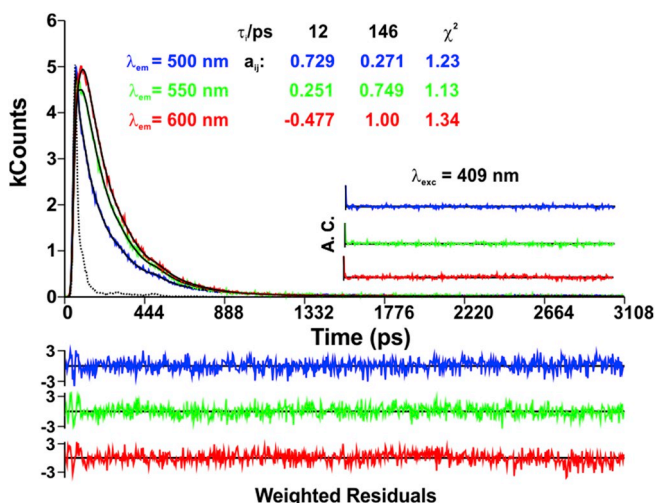$$\lambda_1 \cdot \lambda_2 = k_X k_Y - k_a k_d \tag{11}$$

The pre-exponential factors a_{ij} are the linear combinations of the eigenvector basis set which obey the following initial conditions:

$$a_{11} + a_{12} = 1 \tag{12}$$

$$a_{21} + a_{22} = 0 \tag{13}$$

It is worth noting that application of these initial conditions to the investigated systems is dependent on the excitation wavelength. This means that by using different excitation wavelengths one should expect to obtain different a_{ij} values. Simple manipulation of eqs. (4) and (7), together with eq. (11) and considering the initial conditions given by eqs. (12) and (13), leads to the following relations for the pre-exponential amplitudes (a_{ij}):

$$a_{11} = \frac{k_X - \lambda_2}{\lambda_1 - \lambda_2} \tag{14}$$

$$a_{12} = \frac{\lambda_1 - k_X + k_d}{\lambda_1 - \lambda_2} \qquad (15)$$

$$a_{21} = \frac{k_X - \lambda_1}{\lambda_2 - \lambda_1} \qquad (16)$$

$$a_{22} = \frac{k_X - \lambda_2}{\lambda_1 - \lambda_2} \qquad (17)$$

The system is therefore reduced to 3 unknowns (k_a, k_d, and k_{CT}), to be evaluated from λ_2, λ_1, A and B (eqs. (18) and (19)).

$$A = \frac{a_{12}}{a_{11}} = \frac{k_X - \lambda_1}{\lambda_2 - k_X} \qquad (18)$$

$$B = \frac{a_{22}}{a_{21}} = -1 \qquad (19)$$

which are obtained from the pre-exponential ratio at the emission of LE (A) and CT (B) species/states.

Rearrangement of eq. (18) leads to:

$$k_X = \frac{A\lambda_2 + \lambda_1}{A + 1} \qquad (20)$$

Further manipulation yields:

$$k_a = \frac{A\lambda_2 + \lambda_1}{A + 1} - k_{LE} \qquad (21)$$

and from eq. (11), the following eq. is obtained

$$k_d = \frac{k_X k_Y - \lambda_1 \lambda_2}{k_a} \qquad (22)$$

and finally from eq. (6) one obtains the value of $k_{CT} = k_Y - k_d$.

From the decay parameters, a_{ij} and τ_i and k_{LE} which is the reciprocal of the lifetime of the model compound, here taken as the same of that for indigo (see Ref. [3] with a value of 152 ps), we obtained k_{CT} values in the 3.10–8.30 ns^{-1} for **TRYP** in the protic polar solvents methanol, ethanol and methanol:glycerol (see Table 5).

Noteworthy, is the insignificant change in the decay times going from MeOH to the viscous methanol:glycerol (70:30, v/v) mixture thus excluding the formation of different **TRYP** conformers in the excited state. Indeed, it has been reported that **TRYP** can adopt two conformations when adsorbed in highly oriented pyrolytic graphite, i.e., a planar structure where the nitrogen on the amide moiety is sp^2 hybridized and a non-planar form in which this same nitrogen is sp^3 hybridized [19]. However, and in agreement with our work, in solution it was shown that **TRYP** assumes a planar conformation [19]. Indeed, as suggested by crystallographic studies [67], **TRYP** was computationally modeled in a completely planar conformation, which maximizes the aromaticity and represents the lowest energy conformer.

Data in Table 5 indicates that the rate constant for the formation of the S_1(CT) from the S_1(LE) state, k_a, is higher in methanol but essentially of the same order of magnitude in all solvents. Very interesting is to note the close proximity between the k_a and k_d values for the investigated solvents, which indicates a highly reversible system and a very efficient deactivation of the excited state of **TRYP** as predicted from TDDFT.

3.2.5. Time-resolved femtosecond transient difference absorption spectra (fs-TA)

Additional information on the excited-state deactivation process in **TRYP** was obtained from femtosecond (fs)-transient absorption (TA) data (Table 6).

The time-resolved femtosecond transient difference absorption spectra (fs-TA) for **TRYP** was recorded in aerated MeOH, methanol: glycerol (70:30, v/v) and MeCN solutions in the 340–750 nm range with excitation at 300 nm and 430 nm (see Fig. 5 for MeCN and Figure SI8 for MeOH and methanol:glycerol mixtures). The fs-TA spectra are dominated by strongly overlapped positive broad transient absorption bands in the 350–650 nm range with maxima at ~460 nm in MeOH and in the methanol:glycerol mixture while in MeCN the maxima is at ~470 nm.

The fs-TA data in the 340–750 range show that the decays are well fitted with a sum of three exponential (see Table 6 and Table SI1). The fast decay transients (τ_1) with values in the 2.2–8.9 ps range, which are associated with a negative pre-exponential values when the decays are collected at 465 nm (Table SI1), are not consistent with the solvation dynamics times reported for these solvents [68] and are therefore associated to the S_1(LE) to S_1(CT) state inter-conversion previously described. Indeed, from Table 6 it can be seen that, in general, the intermediate decay components, τ_2, are in good agreement with the fluorescence lifetimes assigned to the decay of the CT state. The longer component (τ_3) although needed to properly fit the decays, comes undefined in fs-TA measurements and is defined from ns-TA experiments (see below).

Nanosecond-microsecond transient absorption spectra, ns-TA, for **TRYP** were also obtained by laser flash photolysis with excitation at 355 nm in degassed MeOH and MeCN solutions (Fig. 6). The observed transient lifetimes were quenched by oxygen and thus are attributed to the triplet excited state absorption. Worth mention that, with the exception of the fs-TA data collected in MeOH and MeOH:glycerol mixture with excitation at 430 nm (which decayed completely within the fs-TA observation time-window), in general, the positive TA bands at higher delay times are in good agreement with the ns-TA bands (see Fig. 5 and SI8-9) and thus are attributed to the excited state triplet-triplet transient absorption.

Noteworthy is the appearance of a new band in the ns-TA spectra in MeCN solution with maxima at ~550 nm (see the spectra obtained at 0.4 µs and 0.6 µs delay times, Fig. 6B) and at 370 nm in MeOH solution (data collected at 4 µs and 10 µs, Fig. 6A).

4. Conclusions

The synthesis of **TRYP** from indigo, through MW irradiation, and a detailed investigation of the excited state deactivation pathways has been undertaken. The results showed that the excited state deactivation

Table 6
Results of the global fit analysis (lifetimes, τ_i) obtained from the time-resolved transient absorption data collected with excitation at 300 nm together (for comparison) with the fluorescence decay times obtained from Picosecond Time-Correlated Single Photon Counting technique for **TRYP** in solvents of different viscosity (η) and dielectric constant (ε) at T = 293 K.
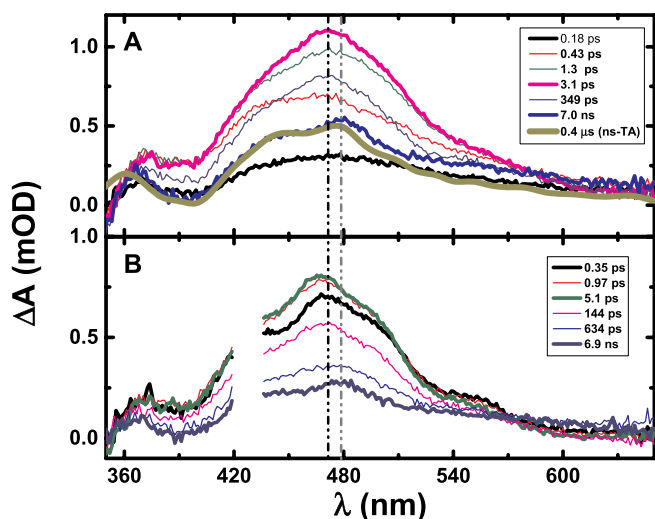
Solvent	η (cP)	ε	$[\tau_1]^a$ (ps)	$[\tau_2]^a$ (ps)	$[\tau_3]^{a,b}$ (µs)	τ_1^a (ps)	τ_2^a (ps)
MeCN	0.345	35.94	8.9	466	1.95	65	499
MeOH	0.593	32.66	3.1	165	51	12	146
MeOH: Glycerol (70:30)	7.700^c	36.70^c	2.2	156	51	17	127

^{a} Decay time values, τ_i, from fs-TA in brackets and the three last values from ps-TCSPC.
^{b} This transient lifetime was fixed in the global analysis to the triplet lifetime obtained by ns-TA.
^{c} For MeOH:Glycerol (70/30) volume ratio data from Ref. [54].

Table 5
Time-resolved data (λ_1, λ_2 and A) and rate constants (k_a, k_d and k_{CT}) recovered the kinetic analysis resulting from Scheme 4.

Solvent	λ_1	λ_2	A	k_a (ns^{-1})	k_d (ns^{-1})	k_{CT} (ns^{-1})
EtOH	3.92	43.14	3.55	27.93	9.45	3.10
MeOH	6.85	80.44	2.70	53.99	19.77	6.94
MeOH:Glycerol (70:30)	7.85	59.27	2.70	38.81	13.43	8.30

Fig. 5. Time-resolved transient absorption data for **TRYP** obtained with excitation at 300 nm (**A**) and 430 nm (**B**) in aerated acetonitrile (MeCN) solutions at T = 293 K. For the data collected with excitation at 430 nm the spectral range 419–436 nm is not shown because it is disturbed by the scattered pump beam. The dashed vertical lines are just meant to be a guideline for the eye. The normalized triplet-triplet absorption spectra collected by ns-TA is presented in (**A**) to show the good agreement with the TA band collected at higher delay times in the fs-TA time-resolved spectra and assign the later to the characteristic triplet-triplet absorption.
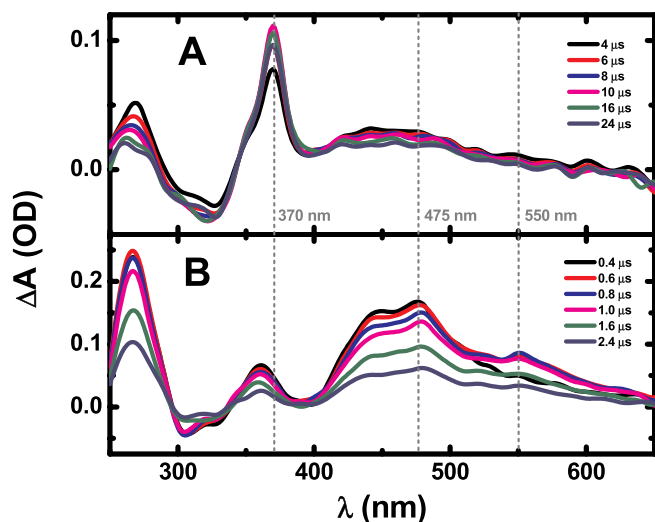
Fig. 6. Room-temperature transient singlet–triplet difference absorption spectra for **TRYP** collected with excitation at 355 nm in degassed methanol (**A**) and acetonitrile (**B**) solutions at T = 293 K.

pathways are remarkably different to those of indigo. Indeed, in contrast to indigo where the $S_1 \leadsto S_0$ internal conversion dominates the excited state deactivation (with more than 99.99% of the quanta loss) in **TRYP** the highly efficient radiationless deactivation channel has a different nature with the formation (detected from longer decay components in fs-TA and ns-TA absorption) of a poorly emissive triplet state (with a phosphorescence quantum yield of 2.7×10^{-3}) and an efficient singlet oxygen sensitization, $\phi_\Delta = 0.77$. From time-resolved fluorescence and fs-TA absorption two clear dominant decay components, τ_1 and τ_2 are observed which is further corroborated on the basis of the existence of LE and CT species from TDDFT. These two species are found with S_1 states of n,π* (CT) character coexisting with a LE state with dominant π,π* character. The inter-conversion, in the excited state, between the CT

and LE species was further investigated and the obtained rate constants found to be on the order of 10^{10} s^{-1} with a reversible process of the same order of magnitude.

Declaration of competing interest

The authors declare that there are no conflicts to declare.

Appendix A. Supplementary data

Supplementary data to this article can be found online at https://doi.org/10.1016/j.dyepig.2019.108125.

Supplementary information

Figures SI1 to SI9 and Table SI1.

References

[1] Seixas de Melo JS. The molecules of colour and art. Molecules with history and modern applications. In: Albini A, Prodi S, editors. Photochemistry. London: RSC; 2020. p. 196–216.
[2] Seixas de Melo JS. The molecules of colour. Photochemistry 2018;45:68–100. The Royal Society of Chemistry.
[3] Pina J, Sarmento D, Accoto M, Gentili PL, Vaccaro L, Galvão A, et al. Excited-state proton transfer in indigo. J Phys Chem B 2017;121(10):2308–18.
[4] Seixas de Melo JS, Rondão R, Burrows HD, Melo MJ, Navaratnam S, Edge R, et al. Spectral and photophysical studies of substituted indigo derivatives in their keto forms. ChemPhysChem 2006;7(11):2303–11.
[5] Volkov VV, Chelli R, Righini R, Perry CC. Indigo chromophores and pigments: structure and dynamics. Dyes Pigments 2020;172:107761.
[6] Pereira RC, Pineiro M, Galvão AM, Seixas de Melo JS. Thioindigo, and sulfonated thioindigo derivatives as solvent polarity dependent fluorescent on-off systems. Dyes Pigments 2018;158:259–66.
[7] Yumusak C, Prochazkova AJ, Apaydin DH, Seelajaroen H, Sariciftci NS, Weiter M, et al. Indigoidine – biosynthesized organic semiconductor. Dyes Pigments 2019; 171:107768.
[8] Rondão R, Seixas de Melo JS. Thio-Mayan-like compounds: excited state characterization of indigo sulfur derivatives in solution and incorporated in palygorskite and sepiolite clays. J Phys Chem C 2013;117(1):603–14.
[9] Rondão R, Seixas de Melo JS, Bonifácio VDB, Melo MJ. Dehydroindigo, the forgotten indigo and its contribution to the color of maya blue. J Phys Chem A 2010;114(4):1699.
[10] He B, Pun AB, Zherebetskyy D, Liu Y, Liu F, Klivansky LM, et al. New form of an old natural dye: bay-annulated indigo (BAI) as an excellent electron accepting unit for high performance organic semiconductors. J Am Chem Soc 2014;136(42): 15093–101.
[11] Jahng Y. Progress in the studies on tryptanthrin, an alkaloid of history. Arch Pharm Res (Seoul) 2013;36(5):517–35.
[12] Honda G, Tosirisuk V, Tabata M. Isolation of an antidermatophytic, tryptanthrin, from indigo plants, polygonum tinctorium and isatis tinctoria. Planta Med 1980;38 (3):275–6.

[13] Hashimoto T, Aga H, Chaen H, Fukuda S, Kurimoto M. Isolation and identification of anti-Helicobacter pylori compounds from *Polygonum tinctorium* lour. J Nat Med 1999;53(1):27–31.

[14] Jao C-W, Lin W-C, Wu Y-T, Wu P-L. Isolation, structure elucidation, and synthesis of cytotoxic tryptanthrin analogues from *Phaius mishmensis*. J Nat Prod 2008;71(7): 1275–9.

[15] Rasmussen L, Lee T, Daves GJ, Schmidt M. Female-to-male sex pheromones of low volatility in the Asian elephant,*Elephas maximus*. J Chem Ecol 1993;19(10): 2115–28.

[16] Tucker AM, Grundt P. The Chemistry of tryptanthrin and its derivatives. Arkivoc 2012:546–69.

[17] Kaur R, Manjal SK, Rawal RK, Kumar K. Recent synthetic and medicinal perspectives of tryptanthrin. Bioorg Med Chem 2017;25(17):4533–52.

[18] Deryabin PI, Moskovkina TV, Shevchenko LS, Kalinovskii AI. Synthesis and antimicrobial activity of tryptanthrin adducts with ketones. Russ J Org Chem 2017; 53(3):418–22.

[19] Novak MJ, Clayton Baum J, Buhrow JW, Olson JA. Scanning tunneling microscopy of indolo[2,1-b]quinazolin-6,12-dione (tryptanthrin) on Hopg: evidence of adsorption-induced stereoisomerization. Surf Sci 2006;600(20):L269–73.

[20] Bhattacharjee AK, Skanchy DJ, Jennings B, Hudson TH, Brendle JJ, Werbovetz KA. Analysis of stereoelectronic properties, mechanism of action and pharmacophore of synthetic indolo[2,1-b]quinazoline-6,12-dione derivatives in relation to antileishmanial activity using quantum chemical, cyclic voltammetry and 3-D-QSAR CATALYST procedures. Bioorg Med Chem 2002;10(6):1979–89.

[21] Kawakami J, Matsushima N, Ogawa Y, Kakinami H, Nakane A, Kitahara H, et al. Antibacterial and antifungal activities of tryptanthrin derivatives. Trans Mater Res Soc Jpn 2011;36(4):603–6.

[22] Filatov AS, Knyazev NA, Shmakov SV, Bogdanov AA, Ryazantsev MN, Shtyrov AA, et al. Concise synthesis of tryptanthrin spiro analogues with in vitro antitumor activity based on one-pot, three-component 1,3-dipolar cycloaddition of azomethine ylides to cyclopropenes. Synthesis 2019;51(3):713–29.

[23] Amara R, Awad H, Chaker D, Bentabed-Ababsa G, Lassagne F, Erb W, et al. Conversion of isatins to tryptanthrins, heterocycles endowed with a myriad of bioactivities. Eur J Org Chem 2019:5302–12.

[24] Matsui M, Morita M, Shibata K, Takase Y. Ozonolysis of indigo. Nippon Kagaku Kaishi 1982;1982(7):1268–9.

[25] Novotná P, Boon JJ, van der Horst J, Pacáková V. Photodegradation of indigo in dichloromethane solution. Color Technol 2003;119(3):121–7.

[26] Nelson AC, Kalinowski ES, Jacobson TL, Grundt P. formation of tryptanthrin compounds upon oxone-induced dimerization of indole-3-carbaldehydes. Tetrahedron Lett 2013;54(50):6804–6.

[27] Abe T, Itoh T, Choshi T, Hibino S, Ishikura M. One-pot synthesis of tryptanthrin by the dakin oxidation of indole-3-carbaldehyde. Tetrahedron Lett 2014;55(38): 5268–70.

[28] Li X, Huang H, Yu C, Zhang Y, Li H, Wang W. Synthesis of tryptanthrins by organocatalytic and substrate Co-catalyzed photochemical condensation of indoles and anthranilic acids with visible light and O₂. Org Lett 2016;18(21):5744–7.

[29] Li H-Y, Chen C-Y, Cheng H-T, Chu Y-H. Exploiting 1,2,3-triazolium ionic liquids for synthesis of tryptanthrin and chemoselective extraction of copper(II) ions and histidine-containing peptides. Molecules 2016;21(10):1355.

[30] Kawakami J, Kikuchi K, Chiba K, Matsushima N, Yamaya A, Ito S, et al. 2-Aminotryptanthrin derivative with pyrene as a FRET-based fluorescent chemosensor for Al³⁺. Anal Sci 2009;25(12):1385–6.

[31] Kawakami J, Soma A, Kikuchi K, Kikuchi Y, Ito S, Kitahara H. 2-Aminotryptanthrin derivative with pyrene as a FRET-based fluorescent chemosensor for metal ions. Anal Sci 2014;30(10):949–54.

[32] Kawakami J, Takahashi M, Ito S, Kitahara H. Photophysical properties of the 2-hydroxytryptanthrin and its sodium salt as near-infrared dyes for fluorescent imaging. Anal Sci 2016;32(2):251–3.

[33] Kawakami J, Tsuiki A, Ito S, Kitahara H. Naphthalene ring-fused 2-aminotryptan-thrin as a fluorescent chemosensor for Al³⁺. Trans Mater Res Soc Jpn 2016;41(1): 131–3.

[34] Kawakami J, Sasagawa M, Ito S. 2-Hydroxy-1-((2-(pyridin-2-yl)hydrazono)methyl) tryptanthrin as a Fluorescent Chemosensor for Metal Ions. Trans Mater Res Soc Jpn 2018;43(3):209–12.

[35] Kawakami J, Kinami Y, Takahashi M, Ito S. 2-Hydroxytryptanthrin and 1-Formyl-2-hydroxytryptanthrin as fluorescent metal-ion sensors and near-infrared fluorescent labeling reagents. Trans Mater Res Soc Jpn 2018;43(2):109–12.

[36] Kawakami J, Kadowaki T, Ikeda M, Habata Y, Ito S, Kitahara H. Spectral characteristics of highly fluorescent 2-(*N,N*-dimethylamino)tryptanthrin. Trans Mater Res Soc Jpn 2016;41(2):143–6.

[37] Kawakami J, Osanai C, Ito S. Fluorescence emission mechanism of three *N,N*-dimethylaminotryptanthrins by density functional theory calculations. Trans Mater Res Soc Jpn 2018;43(5):319–23.

[38] Kawakami J, Kawaguchi H, Kikuchi K, Yamaya A, Ito S, Kitahara H. Fluorescent solvatochromism of 2-aminotryptanthrin. Trans Mater Res Soc Jpn 2013;38(1): 123–5.

[39] Brandão P, Pinheiro D, Seixas de Melo JS, Pineiro M. I2/NaH/DMF as oxidant *trio* for the synthesis of tryptanthrin from indigo or isatin. Dyes Pigments 2020;173: 107935.

[40] Becker RS, Seixas de Melo JS, Maçanita AL, Elisei F. Comprehensive evaluation of the absorption, photophysical, energy transfer, structural, and theoretical properties of α-oligothiophenes with one to seven rings. J Phys Chem 1996;100 (48):18683–95.

[41] Dubois JT, Wilkinson F. Radiative lifetime of triplet biacetyl. J Chem Phys 1963;39 (4):899–901.

[42] Montalti M, Credi A, Prodi L, Gandolfi MT. Handbook of photochemistry. Taylor & Francis Group, LLC; 2006.

[43] Seixas de Melo JS, Pina J, Dias FB, Maçanita AL. Experimental techniques for excited state characterisation. In: Evans RC, Douglas P, Burrow HD, editors. Applied photochemistry. Dordrecht: Springer Netherlands; 2013. p. 533–85.

[44] Martínez CG, Neuner A, Martí C, Nonell S, Braun AM, Oliveros E. Effect of the media on the quantum yield of singlet oxygen (O₂(¹Δg)) production by *9H*-Fluoren-9-one: solvents and solvent mixtures. Helv Chim Acta 2003;86(2):384–97.

[45] Pina J, Seixas de Melo JS, Burrows HD, Maçanita AL, Galbrecht F, Bünnagel T, et al. Alternating Binaphthyl−Thiophene copolymers: synthesis, spectroscopy, and photophysics and their relevance to the question of energy migration versus conformational relaxation. Macromolecules 2009;42(5):1710–9.

[46] Striker G, Subramaniam V, Seidel CAM, Volkmer A. Photochromicity and fluorescence lifetimes of green fluorescent protein. J Phys Chem B 1999;103(40): 8612–7.

[47] Snellenburg JJ, Laptenok S, Seger R, Mullen KM, Van Stokkum I, Glotaran HM. A Java-based graphical user interface for the R package TIMP. J Stat Softw 2012;49 (3).

[48] Riepl HM, Urmann C. Improved synthesis of indirubin derivatives by sequential build-up of the indoxyl unit: first preparation of fluorescent indirubins. Helv Chim Acta 2012;95(8):1461–77.

[49] Pina J, Burrows HD, Becker RS, Dias FB, Maçanita AL, Seixas de Melo JS. Photophysical Studies of α,ω-Dicyano-oligothiophenes NC(C₄H₂S)ₙCN (*n* = 1−6). J Phys Chem B 2006;110(13):6499–505.

[50] Schmidt MW, Baldridge KK, Boatz JA, Elbert ST, Gordon MS, Jensen JH, et al. General atomic and molecular electronic structure system. J Comput Chem 1993; 14(11):1347–63.

[51] Yanai T, Tew DP, Handy NC. A new hybrid exchange–correlation functional using the Coulomb-attenuating method (CAM-B3LYP). Chem Phys Lett 2004;393(1): 51–7.

[52] Maurizio C, Vincenzo B. Time-dependent density functional theory for molecules in liquid solutions. J Chem Phys 2001;115(10):4708–17.

[53] Seixas de Melo JS, Burrows HD, Serpa C, Arnaut LG. The triplet state of indigo. Angew Chem Int Ed 2007;46(12):2094–6.

[54] Levitt JA, Chung P-H, Kuimova MK, Yahioglu G, Wang Y, Qu J, et al. Fluorescence anisotropy of molecular rotors. ChemPhysChem 2011;12(3):662–72.

[55] Reichardt C. Solvatochromic dyes as solvent polarity indicators. Chem Rev 1994;94 (8):2319–58.

[56] Sanjoy Singh T, Mitra S. Fluorescence behavior of intramolecular charge transfer state in *trans*-ethyl p-(dimethylamino)cinamate. J Lumin 2007;127(2):508–14.

[57] Four M, Riehl D, Mongin O, Blanchard-Desce M, Lawson-Daku LM, Moreau J, et al. A novel ruthenium(ii) complex for two-photon absorption-based optical power limiting in the near-IR range. Phys Chem Chem Phys 2011;13(38):17304–12.

[58] Rondão R, Seixas de Melo JS, Voss G. Characterization of the excited states of indigo derivatives in their reduced forms. ChemPhysChem 2010;11(9):1903–8.

[59] Seixas de Melo JS, Moura AP, Melo MJ. Photophysical and spectroscopic studies of indigo derivatives in their keto and leuco forms. J Phys Chem A 2004;108(34): 6975–81.

[60] Seixas de Melo JS, Rondão R, Burrows HD, Melo MJ, Navaratnam S, Edge R, et al. Photophysics of an indigo derivative (keto and leuco structures) with singular properties. J Phys Chem A 2006;110(51):13653–61.

[61] Seixas de Melo JS, Fernandes PF. Spectroscopy and photophysics of 4-and 7-hydroxycoumarins and their thione analogs. J Mol Struct 2001;565:69–78.

[62] El-Sayed MA. Triplet state - its radiative and nonradiative properties. Acc Chem Res 1968;1(1):8–16.

[63] Seixas de Melo JS, Maçanita AL. Three interconverting excited species: experimental study and solution of the general photokinetic triangle by time-resolved fluorescence. Chem Phys Lett 1993;204(5):556–62.

[64] Seixas de Melo JS, Costa T, Miguel MdG, Lindman B, Schillén K. Time-resolved and steady-state fluorescence studies of hydrophobically modified water-soluble polymers. J Phys Chem B 2003;107(46):12605–21.

[65] Seixas de Melo JS, Costa T, Francisco A, Maçanita AL, Gago S, Gonçalves IS. Dynamics of short as compared with long poly(acrylic acid) chains hydrophobically modified with pyrene, as followed by fluorescence techniques. Phys Chem Chem Phys 2007;9(11):1370–85.

[66] Boyce WE, DiPrima RC. Elementary differential equations and boundary value problems. fourth ed. New York: John Wiley & Sons; 1986.

[67] Brufani M, Fedeli W, Mazza F, Gerhard A, Keller-Schierlein W. The structure of tryptanthrin. Experientia 1971;27(11):1249–50.

[68] Horng ML, Gardecki JA, Papazyan A, Maroncelli M. Subpicosecond measurements of polar solvation dynamics: coumarin 153 revisited. J Phys Chem 1995;99(48): 17311–37.